Generation and Detection of Spin Currents in Semiconductor Nanostructures with Strong Spin-Orbit Interaction

Fabrizio Nichele,[1,*] Szymon Hennel,[1] Patrick Pietsch,[1] Werner Wegscheider,[1] Peter Stano,[2,3] Philippe Jacquod,[4] Thomas Ihn,[1] and Klaus Ensslin[1]

[1]*Solid State Physics Laboratory, ETH Zürich, 8093 Zürich, Switzerland*
[2]*RIKEN Center for Emergent Matter Science, 2-1 Hirosawa, Wako, Saitama 351-0198, Japan*
[3]*Institute of Physics, Slovak Academy of Sciences, Dubravska cesta 9, 84511 Bratislava, Slovakia*
[4]*HES-SO, Haute Ecole d'Ingénierie, 1950 Sion, Switzerland*

(Received 14 September 2014; revised manuscript received 28 April 2015; published 18 May 2015)

Storing, transmitting, and manipulating information using the electron spin resides at the heart of spintronics. Fundamental for future spintronics applications is the ability to control spin currents in solid state systems. Among the different platforms proposed so far, semiconductors with strong spin-orbit interaction are especially attractive as they promise fast and scalable spin control with all-electrical protocols. Here we demonstrate both the generation and measurement of pure spin currents in semiconductor nanostructures. Generation is purely electrical and mediated by the spin dynamics in materials with a strong spin-orbit field. Measurement is accomplished using a spin-to-charge conversion technique, based on the magnetic field symmetry of easily measurable electrical quantities. Calibrating the spin-to-charge conversion via the conductance of a quantum point contact, we quantitatively measure the mesoscopic spin Hall effect in a multiterminal GaAs dot. We report spin currents of 174 pA, corresponding to a spin Hall angle of 34%.

DOI: 10.1103/PhysRevLett.114.206601 PACS numbers: 72.25.Dc, 72.25.Hg, 73.23.−b, 75.76.+j

The generation and detection of spin currents in nanostructures is the central challenge of semiconductor spintronics. On the one hand, spin injection cannot be easily achieved by coupling semiconductors to ferromagnets [1] because of the lack of control over material interfaces [2]. On the other hand, magnetoelectric alternatives exploiting the celebrated spin Hall effect (SHE) [3,4], have delivered only qualitative measurement protocols in transport experiments [5]. Alternatively to all-electrical setups, spin polarizing the current through a quantum point contact (QPC) with a magnetic field allows a quantitative control over spin current generation and detection at the nanoscale [6–8]. The latter approach requires, however, such high magnetic fields (6–8 T), that the desired magnetoelectric effects are either suppressed or totally altered.

This Letter reports two major advances of nanoscale semiconductor spintronics. Namely, we develop novel experimental methods to *electrically generate* and *quantitatively measure* spin currents in a two-dimensional semiconductor nanostructure.

It is predicted that charge currents flowing through spin-orbit interaction (SOI)-coupled nanostructures are generically accompanied by spin currents, if the spin-orbit time is shorter than the electron dwell time [9–12]. This spin current generation mechanism is purely electrical and based on the mesoscopic SHE (MSHE) [9,10], where the electronic orbital dynamics in chaotic nanostructures cooperates with the SOI to make transport spin dependent. We will consider an open three-terminal quantum dot as represented in Fig. 1(a), where each lead i is a QPC carrying N_i spin degenerate modes. Running a charge current I between terminals 1 and 2, a spin current in all terminals, including 3, is expected due to the MSHE.

For a weak SOI, the spin currents' amplitude fluctuates from sample to sample with zero average. For cavities with a strong SOI, geometric correlations between the spin and

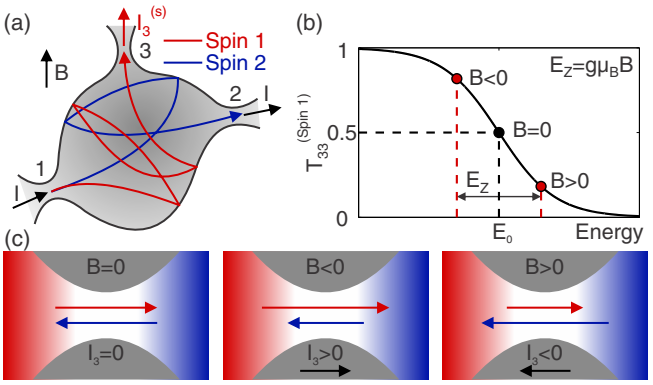

FIG. 1 (color online). (a) Schematic of the system used to generate spin currents. Charge currents are depicted as black lines, spin currents are depicted as red and blue lines. (b) Energy dependent, spin sensitive, transmission probability of QPC_3. At zero field the transmission is tuned to 1/2. A positive (negative) field suppresses (enhances) the transmission probability of one spin eigenstate. (c) Representation of spin and charge currents in QPC_3 as a function of magnetic field. The net charge current in QPC_3 varies with the magnetic field.

the orbital electronic dynamics lead to spin currents with large, predictable nonzero average values [13]. In the latter case, the spin currents' amplitude is determined by the nanostructure geometry and the SOI strength. This particular mechanism renders spin currents robust against decoherence and allows us to differentiate them from mesoscopic fluctuations. This is essential for spintronics applications, where spin currents must be reproducible regardless of the microscopic details of the sample.

To detect and measure the spin currents described above, we employ the scheme of Ref. [14], based on the magnetic field parity of the voltage behind a QPC. With reference to Fig. 1(a), we are interested in the spin current $I_3^{(S)}$ emitted from QPC_3. The energy dependent transmission probability of QPC_3, $T_{33}^{(s)}$, is shown in Fig. 1(b). At zero field, QPC_3 is tuned to a conductance of e^2/h by a suitable gate voltage, corresponding to a spin-independent transmission probability of one half. A weak in-plane magnetic field B modifies the electrons' kinetic energy via Zeeman coupling, selectively increasing or decreasing the transmission probability according to the spin eigenstate and magnetic field sign. For simplicity, we assume $I_3^{(S)}$ to be a pure spin current at $B = 0$, arising as two counterpropagating and inversely spin-polarized charge currents of equal magnitude, as schematically shown in Fig. 1(c), where arrows indicate current amplitude and colors spin polarization. A magnetic field affects the QPC spin dependent transmission probability, enhancing one of the two charge currents and suppressing the other. The result is the flow of a net charge current I_3 in the QPC. The sign of I_3 reverses by reversing the magnetic field sign. Note that the net spin current remains constant in the three situations depicted in Fig. 1(c).

By operating QPC_3 as a floating probe, the charge current I_3 is constantly fixed to zero. In this case, the presence of a spin current $I_3^{(S)}$ in the QPC reflects itself in an antisymmetric component of the voltage behind it: $V_3(B) \neq V_3(-B)$. Remarkably, theory predicts that the zero-field derivative of the measured voltage, $\partial_B V_3$, is proportional to the spin current $I_3^{(S)}$ polarized along the applied magnetic field. The proportionality coefficient between the spin-to-charge signal $\partial_B V_3$ and $I_3^{(S)}$ is given by the QPC g factor and its energy sensitivity $\hbar\omega$ measured at $N_3 = 0.5$ [14]:

$$I_3^{(S)} = \frac{e^2}{h}\frac{2\hbar\omega}{\pi g \mu_B}\partial_B V_3. \quad (1)$$

More generally, for $N_3 \leq 1$ the presence of the spin current still reflects itself in a finite spin-to-charge signal whose amplitude is directly proportional to the detector normalized transconductance: $\partial_B V_3 \propto \partial_V G_3/G_3$. For $N_3 = 0.5$ it results in $\partial_V G_3/G_3 = -\pi/\hbar\omega$. Details about the derivation of this proportionality and Eq. (1) are reported in the Supplemental Material [15]. Equation (1) not only allows us to detect the presence of a spin current flowing in QPC_3, but also to quantitatively measure and express it in units of ampere, giving the difference in currents carried by electrons with opposite polarization. Given the large SOI of our system, the measurement process requires only weak magnetic fields that do not affect the generated spin currents. We note that our approach is restricted to the linear response regime, and to terminal 3 being a weak probe, i.e., $N_3 \leq 1 \ll N_1, N_2$. The measurement protocol described here is independent of the spin current generation mechanism. In particular, the detection method can be used to measure spin currents of other origin.

Motivated by the theory above, we study a three-terminal chaotic cavity embedded in a p-type GaAs two-dimensional hole gas (2DHG) with a strong Rashba SOI. Our sample, shown in Fig. 2(a), lacks any spatial symmetry and consists of three leads and five in-plane gates, named QPC_i and g_j, respectively. The gates g_4 and g_5, colored in blue, tune the conductance of QPC_3 with little influence on the dot average

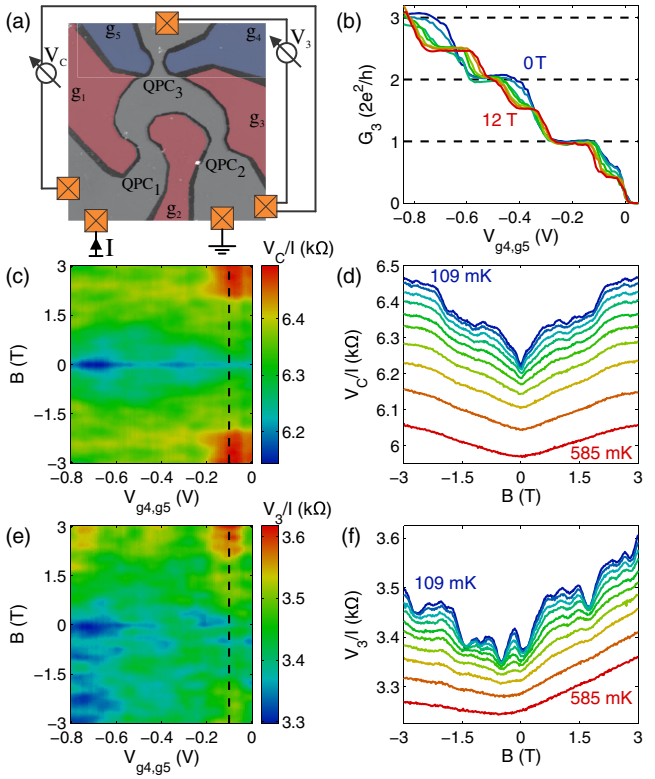

FIG. 2 (color online). (a) Atomic force micrograph of our sample, where dark lines indicate insulating trenches. The frame size is 5×5 μm^2. (b) QPC_3 conductance as a function of the voltage applied to g_4 and g_5, for different values of magnetic field. (c) Cavity four-terminal resistance as a function of the voltage applied to g_4 and g_5 and magnetic field. (d) Line cut of (c) along the dashed line for different temperatures. (e) V_3/I as a function of the voltage applied to g_4 and g_5 and magnetic field. (f) Line cut of (e) along the dashed line for different temperatures.

conductance. The gates g_1, g_2, and g_3, depicted in red, tune the conductance of QPC_1 and QPC_2, and also affect the dot shape. The lateral extent of the cavity is about 2 μm, the hole mean free path $l_e = 4.8$ μm, and the spin-orbit length $l_{SO} = 36$ nm [15]. Spin rotational symmetry is then completely broken and, with such a strong SOI, our cavity is in the so-called spin chaos regime [13]. Unless differently stated, a charge current I flows from terminal 1 to terminal 2, while terminal 3 is connected to a high impedance voltage amplifier and is used to measure spin currents.

To measure the spin current in terminal 3, we first extract the detector electric and magnetic sensitivity via a standard QPC characterization. Figure 2(b) shows the detector conductance G_3 as a function of side gate voltage for different values of a magnetic field aligned with the QPC_3 axis. The three well-developed plateaus visible at zero field split at finite field. The zero field slope and the finite field splitting give, respectively, $\partial_V G_3$ and the g factor [15].

After the detector calibration, QPC_3 is operated as a voltage probe. The spin current measurement is performed running an ac current ($I = 4$ nA unless stated otherwise) between terminals 1 and 2, and measuring the magnetic dependence of the voltages V_C and V_3 as defined in Fig. 2(a). The magnetic field is applied in-plane, to minimize its orbital effects, and aligned with the detector axis (unless stated otherwise). The finite zero field derivative $\partial_B V_3$, and its correlation with $\partial_V G_3/G_3$, indicates the presence of the spin current $I_3^{(S)}$.

Figures 2(c) and 2(e) show the resistances $R_C = V_C/I$ and V_3/I as a function of B and the voltage applied to g_4 and g_5. Panels (d) and (f) show line cuts along the dashed lines of Figs. 2(c) and 2(e), respectively, for different temperatures. These line cuts are taken for $N_3 = 0.5$. On top of a smooth background, higher frequency conductance fluctuations (CFs) appear at low temperatures. The cavity resistance R_C is symmetric upon magnetic field reversal both in the slowly varying background and in the CFs, as expected from a two-terminal measurement in the linear regime [21]. V_3 is, on the contrary, strongly asymmetric. We first address the slowly varying background of $V_3(B)$. We will discuss the nature of the CFs below.

Large CFs do not allow us to measure meaningful voltage asymmetries at small magnetic fields. We therefore average them out by a linear regression of $V_3(B)$ in a magnetic field range between -1 T and 1 T. The chosen range is an optimal compromise between not sufficient CFs averaging at small fields and unwanted changes of the spin current at large fields. This interval includes at least six CFs, and we carefully checked that the averaged voltage asymmetry only weakly depends on the precise magnetic field range used for the analysis.

The detector voltage asymmetry extracted in this way is plotted in Fig. 3 (markers) together with the detector transconductance. We normalize the detector voltage by the constant cavity current I and show the detector

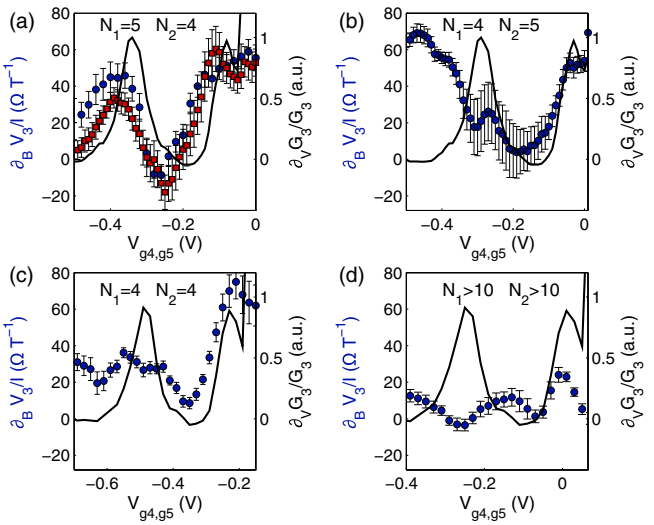

FIG. 3 (color online). (a)–(d) Comparison between $\partial_B V_3/I$ (markers) and $\partial_V G_3/G_3$ (solid line) as a function of the side gate voltage for a different number of modes in QPC_1 and QPC_2, as indicated in each subfigure. Dots and squares in (a) represent two identical measurements performed in different cooldowns [22].

transconductance in arbitrary units. Panels (a)–(d) represent different cavity configurations, with different N_1 and N_2 as indicated in every subfigure. Despite the large error bars introduced by the CFs, in Figs. 3(a), 3(b), and 3(c) we observe what theory anticipates: a correlation of the two quantities below the last detector conductance step (right-hand side of each subfigure) and disappearance of this correlation beyond the first plateau (left-hand side of each subfigure). This is the key observation from which we conclude that we measure a spin current. Where the detector is most energy sensitive, we observe useful signals with $\partial_B V_3/I \approx 70$ ΩT^{-1}, with a typical background of 20 ΩT^{-1}. The latter value was also typically observed for $N_1, N_2 > 6$, as shown in Fig. 3(d), where the voltage asymmetry is uncorrelated with the transconductance. This is expected due to suppression of spin currents by energy averaging when many modes contribute to transport. In the following we give further evidence supporting the spin current origin of the observed voltage asymmetry.

To confirm the spin related nature of our signal, we exploit a key ingredient for the spin-to-charge conversion: the magnetic field sensitivity of the detector QPC. A detector with zero g factor should result in a vanishing voltage asymmetry, regardless of the spin current intensity. We confirmed this prediction in the two ways shown in Fig. 4. In Fig. 4(a) we modified the measurement scheme such that the current flows from terminal 1 to 3, while terminal 2 is used as the detector. The latter is characterized in Ref. [23], and the first mode shows $g = 0$. As expected, we observe a vanishing voltage asymmetry for $N_2 \to 0$ for two different cavity shapes (dots and squares, respectively). As yet an additional test, we kept the measurement scheme as in Fig. 2(a), but rotated the sample by 90° in the 2DHG

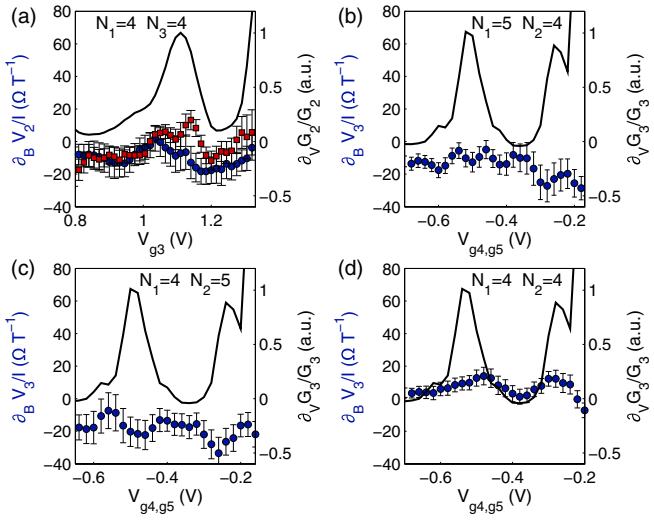

FIG. 4 (color online). (a) Comparison between $\partial_B V_2/I$ acquired with two different cavity shapes (dots and squares) both having $N_1 = N_3 = 4$ and $\partial_V G_2/G_2$ (solid line) as a function of the voltage applied to g_3. The electrical setup was modified to use QPC_2 as detector. (b), (c), and (d) as in Fig. 3 but with the magnetic field aligned perpendicularly to QPC_3.

plane, to have the magnetic field perpendicular to QPC_3. Along this direction, the g factor vanishes for all modes [15], which is a well-known anisotropy of p-type QPCs [23,24]. The latter is a particularly powerful approach as it leaves the spin current unaltered and only suppresses the spin-to-charge conversion efficiency. In Figs. 4(b), 4(c), and 4(d) we show three of such measurements for the same mode configurations as in Figs. 3(a), 3(b), and 3(c). In all the three cases, the voltage asymmetry is comparable to the background level of Fig. 3 and uncorrelated to the detector transconductance, proving the importance of a magnetic field sensitive measurement lead for observing an asymmetric voltage signal.

The spin-to-charge signal shown in Fig. 3 reflects a robust property of the system and is not linked to CFs. The CFs are phase coherent effects originating from electrostatic cavity shape distortion and magnetic flux penetration [25], or from a purely in-plane field as a consequence of the asymmetric and finite-width confinement potential [26]. We carefully checked that our results do not depend on the CFs' pattern first by changing g_1, g_2, and g_3 while keeping N_1 and N_2 constant, second by applying a strong voltage asymmetry on g_4 and g_5. In both cases, the CFs are completely changed without a significant modification of the voltage asymmetry extracted by averaging. Additionally, Fig. 3(a) includes a measurement performed during a different cooldown (squares) [22]. Despite the completely different CFs' fingerprint, an identical voltage asymmetry is obtained, proving the robustness of the measured effect. As visible in Fig. 2(f), coherent contributions are almost entirely suppressed at $T = 530$ mK, which is a standard temperature scale for the disappearance of coherent effects in quantum dots with few open channels [27]. The average signal is, on the other hand, more resistant to temperature increases because of its diffusion-like origin [13]. We performed additional analysis of the temperature and charge current amplitude dependence of the spin-to-charge signal. These measurements, reported in the Supplemental Material [15], confirm the distinct nature of CFs and the spin-to-charge signal, as well as the fact that the spin-to-charge signal is a linear effect.

So far, we discussed the presence of a robust spin current in QPC_3 visible from the slowing varying background of $\partial_B V_3/I$. As discussed in the context of the MSHE, CFs might also reflect the presence of mesoscopic spin CFs [9–12]. Although the CFs occasionally show a finite zero field slope [see Fig. 2(f)], it was not possible to univocally assign them to spin related or orbital effects, not considered in Ref. [14]. In particular, we could not test the QPC_3 transmission dependence of $\partial_B V_3/I$ for single CFs due to the influence of g_4 and g_5 on the cavity shape.

We now evaluate the spin current amplitude for $N_3 = 0.5$. With the measured detector sensitivity $\hbar\omega = 0.46$ meV, its g factor $g = 0.27$ and the typical voltage asymmetry of $\partial_B V_3/I = 60\ \Omega\mathrm{T}^{-1}$, Eq. (1) gives $I_3^{(S)} = 174$ pA. We compare this value with theoretical predictions on geometrical correlation induced spin currents. The spin transmission of QPC_3, calculated for a three-terminal cavity in the spin chaos regime, is [13]

$$\langle T_{13}^{(S)} \rangle = \mathcal{C} \frac{1+2\xi}{2 l_{\mathrm{SO}} k_F} \frac{N_1 N_3}{N_1 + N_2 + N_3} \approx 0.137 \times \mathcal{C}. \quad (2)$$

To evaluate this expression we used $\xi = 1$, appropriate for a ballistic dot, $N_1 = N_2 = 4$, $N_3 = 0.5$. $\mathcal{C}$ is a system specific prefactor, of order unity. Neglecting spin flips caused by QPC_3 itself, the expected spin current is

$$I_3^{(S)} \approx \frac{e^2}{h} \langle T_{13}^{(S)} \rangle (V_1 - V_2) = \mathcal{C} \times 134\ \mathrm{pA} \quad (3)$$

for a charge current of 4 nA. The very good agreement with our measurement further supports the interpretation that our signal goes beyond a mere spin current detection, but provides a quantitatively reliable magnitude. As shown by Eq. (2), the spin conductance depends on N_3, allowing larger spin currents to be generated by opening QPC_3 further. However, since the detection scheme requires $N_3 = 0.5$, we could not probe this scenario.

Similarly to bulk materials, the spin-to-charge conversion efficiency of the cavity can be expressed via the spin Hall angle Θ, defined as the ratio between spin and charge current densities. In our case we get $\Theta = (I_3^{(S)}/N_3)/(I/N_2) \approx 34\%$, independent on N_3 for $N_3 \ll N_1, N_2$. This efficiency is substantially higher than any reported for semiconductors [4], making this system interesting for future semiconductor spintronics applications.

We acknowledge Christian Gerl for growing the wafer structure. The authors wish to thank the Swiss National Science Foundation via NCCR QSIT "Quantum Science and Technology" for financial support.

*Present Address: Center for Quantum Devices, Niels Bohr Institute, University of Copenhagen, 2100 Copenhagen, Denmark. fnichele@phys.ethz.ch; http://www.nanophys.ethz.ch

[1] G. Schmidt, D. Ferrand, L. W. Molenkamp, A. T. Filip, and B. J. van Wees, Phys. Rev. B **62**, R4790 (2000).
[2] S. Sharma, A. Spiesser, S. P. Dash, S. Iba, S. Watanabe, B. J. van Wees, H. Saito, S. Yuasa, and R. Jansen, Phys. Rev. B **89**, 075301 (2014).
[3] M. I. D'yakonov and V. I. Perel', JETP Lett. **13**, 467 (1971).
[4] T. Jungwirth, J. Wunderlich, and K. Olejnik, Nat. Mater. **11**, 382 (2012).
[5] C. Brüne, A. Roth, E. G. Novik, M. Konig, H. Buhmann, E. M. Hankiewicz, W. Hanke, J. Sinova, and L. W. Molenkamp, Nat. Phys. **6**, 448 (2010).
[6] R. M. Potok, J. A. Folk, C. M. Marcus, and V. Umansky, Phys. Rev. Lett. **89**, 266602 (2002).
[7] S. K. Watson, R. M. Potok, C. M. Marcus, and V. Umansky, Phys. Rev. Lett. **91**, 258301 (2003).
[8] S. M. Frolov, A. Venkatesan, W. Yu, J. A. Folk, and W. Wegscheider, Phys. Rev. Lett. **102**, 116802 (2009).
[9] W. Ren, Z. Qiao, J. Wang, Q. Sun, and H. Guo, Phys. Rev. Lett. **97**, 066603 (2006).
[10] J. H. Bardarson, I. Adagideli, and P. Jacquod, Phys. Rev. Lett. **98**, 196601 (2007).
[11] Y. V. Nazarov, New J. Phys. **9**, 352 (2007).
[12] J. J. Krich and B. I. Halperin, Phys. Rev. B **78**, 035338 (2008).
[13] I. Adagideli, P. Jacquod, M. Scheid, M. Duckheim, D. Loss, and K. Richter, Phys. Rev. Lett. **105**, 246807 (2010).
[14] P. Stano and P. Jacquod, Phys. Rev. Lett. **106**, 206602 (2011).
[15] See Supplemental Material at http://link.aps.org/supplemental/10.1103/PhysRevLett.114.206601 for material and methods, temperature and current dependence studies, and a theoretical treatment of the spin-to-charge conversion effect, which includes Refs. [16–20].
[16] F. Nichele, A. N. Pal, R. Winkler, C. Gerl, W. Wegscheider, T. Ihn, and K. Ensslin, Phys. Rev. B **89**, 081306 (2014).
[17] R. Winkler, *Spin-Orbit Coupling Effects in Two-Dimensional Electron and Hole Systems*, Springer Tracts in Modern Physics Vol. 191 (Springer-Verlag, Berlin, 2003).
[18] M. Büttiker, Phys. Rev. B **41**, 7906 (1990).
[19] C. Rössler, S. Baer, E. de Wiljes, P.-L. Ardelt, T. Ihn, K. Ensslin, C. Reichl, and W. Wegscheider, New J. Phys. **13**, 113006 (2011).
[20] P. Stano, J. Fabian, and P. Jacquod, Phys. Rev. B **85**, 241301(R) (2012).
[21] H. B. G. Casimir, Rev. Mod. Phys. **17**, 343 (1945).
[22] For a direct comparison, we horizontally shifted the red curve to account for the different pinch-off voltage of QPC_3 in this cooldown.
[23] F. Nichele, S. Chesi, S. Hennel, A. Wittmann, C. Gerl, W. Wegscheider, D. Loss, T. Ihn, and K. Ensslin, Phys. Rev. Lett. **113**, 046801 (2014).
[24] A. Srinivasan, L. A. Yeoh, O. Klochan, T. P. Martin, J. C. H. Chen, A. P. Micolich, A. R. Hamilton, D. Reuter, and A. D. Wieck, Nano Lett. **13**, 148 (2013).
[25] C. Beenakker and H. van Houten, in *Semiconductor Heterostructures and Nanostructures*, edited by H. Ehrenreich and D. Turnbull (Academic Press, New York, 1991), Vol. 44, pp. 1–228.
[26] D. M. Zumbühl, J. B. Miller, C. M. Marcus, V. I. Fal'ko, T. Jungwirth, and J. S. Harris, Phys. Rev. B **69**, 121305 (2004).
[27] A. G. Huibers, J. A. Folk, S. R. Patel, C. M. Marcus, C. I. Duruöz, and J. S. Harris, Phys. Rev. Lett. **83**, 5090 (1999).